RSC Advances

ROYAL SOCIETY OF CHEMISTRY

www.rsc.org/advances

Fluorinated anthracene derivatives as deep-blue emitters and host materials for highly efficient organic light-emitting devices

Lu Li, Bo Jiao*, Yue Yu, Lin Ma, Xun Hou and Zhaoxin Wu*

Key Laboratory for Physical Electronics and Devices of the Ministry of Education, Xi'an Jiaotong University, Xi'an 710049, People's Republic of China

Abstract

Novel fluorinated anthracene based deep-blue-emitting molecules namely 9,10-Bis-(n'-fluoro-biphenyl-3-yl)-anthracene (nF-DPAs) have been designed and synthesized by a Suzuki cross-coupling reaction. The influence of substitution position of fluorination electron-withdrawing group on the energy levels and photophysical properties of nF-DPAs was studied by experiment and density functional theory (DFT). Organic light-emitting devices (OLEDs) using nF-DPAs as non-doped emitter exhibit bright deep blue electroluminescence with Commisssion Internationale de L'Eclairage (CIE) coordinates of (0.15, 0.09) for 2F-DPA, (0.15, 0.09) for 3F-DPA, and (0.15, 0.07) for 4F-DPA, respectively. Furthermore, it was demonstrated that these nF-DPAs serve as excellent host material for 4,4' -Bis[4-(di-p-tolylamino)styryl]biphenyl (DPAVBi). Especially, OLEDs using 2F-DPA as the fluorescent host exhibit pure blue emission with CIE coordinates of (0.15, 0.30), high luminance over 20 000 cd m^{-2}, high current efficiency of 9.6 cd A^{-1}, and high external quantum efficiency of 5.2%. Our new fluorinated derivatives show potential applications for highly efficient blue OLEDs.

** Email Addresses: bojiao@mail.xjtu.edu.cn, zhaoxinwu@mail.xjtu.edu.cn*

Corresponding authors Tel:+86 29 82664867

1. Introduction

Organic light-emitting devices (OLEDs) have attracted much scientific and commercial interest in recent years because of their potential application in full-color displays and lighting applications.[1–3] For full-color display and white lighting, the three primary colors, red (R), green (G), and blue (B) are essential. However, progress in highly efficient blue OLEDs is far behind its counterparts of green/red OLEDs, due to the difficulty in developing blue-emitting materials with a high efficiency, color purity, and long operation time. Deep-blue emitters with a high quantum efficiency are needed to effectively reduce power consumption and to increase the color gamut of full-color OLEDs. Despite many relevant studies related to blue phosphorescent OLEDs (PhOLEDs) have been reported, realization of high efficiency and long lifetime blue phosphorescent devices is still difficult because of the limitation of host materials with suitable triplet level. Hence, development of blue fluorescent emitters with high colour purity and high efficiency is still a crucial issue for full-color display application.[4–6] It is well known that host-dopant system can significantly avoid concentration quenching of fluorescence molecular and improve device performance, such as efficiency, color purity, as well as operational lifetime.[7] Various host materials for blue emitting OLEDs have been reported to date, such as 2-tert-buty-9,10-bis-(beta-naphthyl)-anthracene (TBADN) and 4,4'-bis(2,2'-diphenylvinyl)-1,1'-biphenyl (DPAVBi) .[8-18] However, novel blue host materials with good thermal and morphological stabilities are still desirable.

Anthracene derivatives possessing excellent photoluminescence (PL) and electroluminescence (EL) properties have been studied intensively to develop efficient blue-emitting materials.[19-26] Unfortunately, 9,10-diphenylanthracene (DPA) tends to crystallize in the solid state making it incapable of providing a homogeneous film in device fabrication, resulting in grain boundaries or pin holes that lead to current leakage. A lot of works have been done to improve the film formation property of DPA by adding special functional groups, such as pyridine, carbazole *et al.*[27-29] A serious drawback, as exemplified by DPA and its derivatives, is that their fluorescence

in the solid state are easily quenched.

Fluorination has been used in the past decade as a route to improve the electron transport in small molecular or polymer because of its strong electron-withdrawing ability.[30-35] The C–H/F interactions, similar to hydrogen bonds, play an important role in the solid state organization of fluorine compounds bearing both C–F and C–H bonds, forming a typical π-stack arrangement which enhances the charge carrier mobility.[33,34,36, 37]

In this work, we designed and synthesized a series new amorphous fluorinated anthracene derivatives named nF-DPAs for blue OLEDs application. For OLEDs based on non-doped nF-DPAs emitter, saturated deep-blue emission with CIE_y coordinate less than 0.1 was achieved. For OLEDs using DPAVBi as dopant and 2F-DPA as the fluorescent, high current efficiency of 9.6 cd A^{-1}, and an external quantum efficiency of 5.2% were demonstrated, which indicates great potential applications for highly efficient blue OLEDs.

2. Results and discussion

2.1 Synthesis, structural characterization and theoretical computation

Scheme 1 illustrates the synthetic approach to nF-DPAs. Anthraquinone reacted with (3-bromophenyl) lithium, which was synthesized from 3-bromo-iodobenzene and n-butyllithium, to form 9,10-bis(3-bromophenyl)anthracene. Then 9,10-bis(3-bromophenyl) anthracene reacted with fluorinated phenylboronic acid via a palladium-catalyzed Suzuki coupling reaction to form the desired product, nF-DPA.[29] After purification by column chromatography and recrystallization, these newly synthesized nF-DPAs were purified further by train sublimation at a reduced pressure below 10^{-3} Pa and fully characterized with ^{1}H NMR and elemental analysis.

Theoretical calculations on the electronic states of nF-DPAs were carried out at the DFT//B3LYP/6-31G level in the Gaussian 03 program. As shown in **Fig 1**, both HOMO and LUMO are mainly located on the anthracence core in nF-DPAs, which results in similar charge-transfer integrals for electrons and holes. The calculated HOMOs and LUMOs of all the nF-DPA are listed in **Table 1**. The HOMO and

LUMO of 2F-DPA are the highest and 4F-DPA are the lowest among these three materials. It can be deduced that the fluoride atom at *para*-position on the phenyl ring in 4F-DPA may exhibit the strongest electron-withdrawing.

2.2 Thermal properties

The thermal properties of nF-DPAs were determined by differential scanning calorimetry (DSC) and thermogravimetric analysis (TGA) are listed in **Fig 2** and **Table 1**. The glass-transition temperature (T_g) of compounds 2F-DPA, 3F-DPA, 4F-DPA were determined to be 117, 112, 119 ^{o}C. Compared with similar pyridine-substitution DPA derivative, whose glass-transition temperature are typically less than 100 ℃, our nF-DPAs exhibit better thermal stability[27]. Their thermal-decomposition temperatures (T_d, corresponding to 5% weight loss) were determined to be 385 ^{o}C. Based on the thermal stability of these compounds, homogeneous and stable amorphous thin films of these compounds could be achieved by vacuum deposition, which matches the basic requirement for host emitters used in OLEDs.

2.3 Photophysical properties

The photophysical properties of nF-DPAs were investigated by means of electronic absorption and steady state photoluminescence (PL) spectra for both dilute solutions in dichloromethane and the solid films on quartz plates. The data are summarized in **Table 1** and **Fig 3**. We assign in solutions the absorption bands of all compounds in the region from 290 to 320 nm to the n–π* transition of the peripheral functional groups.[38] The peaks at 340, 355, 375, 395 nm is attributed to π-π* transition, which is typical absorption of anthracene.[39] For the thin solid film condition, as shown in **Fig. 3(b)** and **Table 1,** a red shift of 5 nm was detected in the absorption spectrum of nF-DPAs in comparison with that in the solution, which may be caused by the difference in dielectric constant of the environment.[40] The optical band gap values (E_g^{opt}, eV) for nF-DPAs were determined from their absorption onset potential edge. As shown in Table 1, these value 3.0 eV.

The compounds are highly emissive in dichloromethane solution with the emission maxima being closely grouped and falling in the deep-blue region (433, 461

nm). In films the PL spectra peaks at 421, 440 nm, it's about 12 and 21 nm blue shifts. This result may also be attributed to the aforementioned solid state packing force which prohibits the electron-vibration coupling between the fluorophenyl substituent and the anthracene photoactive unit. [41]

The fluorescence quantum yields ($\Phi_{f\text{-}sol}$) of the nF-DPAs in dilute CH_2Cl_2 solution were determined by using quinine sulfate as standard (Φ_f = 0.56 in 1.0 M H_2SO_4 solution) at room temperature. In solution, the $\Phi_{f\text{-}sol}$ of compounds 2F-DPA, 3F-DPA, 4F-DPA, and TBADN were determined to be 0.49, 0.52, 0.51 and 0.24 respectively.[42] The $\Phi_{f\text{-}sol}$ results indicates that nF-DPAs exhibit better emission ability than the TBADN. Typically, it was believe that the molecule aggregate state may induce significant influence on their emission property in film state.[43] Therefore, to understand the influence of molecule aggregation in film on the emission performance of nF-DPAs, the fluorescence quantum yields in film state ($\Phi_{f\text{-}film}$) for nF-DPAs and TBADN were measured. The $\Phi_{f\text{-}film}$ of 2F-DPA. 3F-DPA. 4F-DPA, TBADN films were determined to be 0.36, 0.41, 0.38 and 0.18, respectively. The shifting trend of the $\Phi_{f\text{-}film}$ of nF-DPAs film coincides very well with the $\Phi_{f\text{-}sol}$ of nF-DPAs, and the $\Phi_{f\text{-}film}$ value is slightly lower than the $\Phi_{f\text{-}sol}$ value for the same material, which indicates the influence of the molecule aggregation in film state on the emission performance of nF-DPAs is rather small and can be neglected.

2.4 Electrochemical properties

Cyclic voltammetric (CV) studies were performed to calculate the HOMO and LUMO values for the nF-DPAs (**Fig 4**). The oxidation and reduction CV experiments were carried out in solutions of 0.1 M supporting electrolyte (n-Bu_4NPF_6) and 1 mM substrate in dry dichloromethane and acetonitrile, respectively, under a nitrogen atmosphere using ferrocene as an internal standard. All compounds exhibit an oxidation wave at potentials higher than that observed for ferrocene. The HOMO energy levels were estimated from the onset of oxidation potentials as summarized in **Table 1**. The values of the HOMOs for nF-DPAs thus calculated are between -5.72 and -5.82 eV. Same as the results of calculation, 4F-DPA, with a *mono*-F substituent at the *para*-position, has a slightly lower HOMO level (-5.82 eV) than that at the

ortho-position (-5.72 eV) or *meta*-position (-5.79 eV). From the HOMO values and the optical band gap energies (E_g^{opt}) available from the UV-vis spectra, the LUMO energies for the nF-DPA were calculated to be in the range -2.72 eV to -2.82 eV.

2.5 Electroluminescent properties

To evaluate carrier-transport properties of nF-DPA, hole-only and electron-only devices were fabricated. The configuration of hole-only device and electron-only devices are indium tinoxide (ITO) / molybdenum trioxide (MoO_3) (5 nm)/ 4,4'-N,N'-bis[N-(1-naphthyl)-N-phenylamino]biphenyl (NPB) (50 nm)/nF-DPAs (50 nm)/NPB (50 nm)/MoO_3 (5 nm)/Al (100 nm), and ITO/ 4,4'-N,N'-bis[N-(1-naphthyl)-N-phenylamino]biphenyl (TPBi) (20 nm)/nF-DPAs (50 nm)/TPBi (20 nm)/Al (100 nm), respectively. TBADN based hole-only device and electron-only device with same structures were also fabricated as control devices. The current density-voltage characteristics of these hole-only devices and electron-only devices are shown in **Fig. 5(a)** and **5(b)**, respectively. Just as shown in **Fig. 5(a)**, among these three material of 2F-DPA, 3F-DPA and 4F-DPA, 2F-DPA exhibits the best hole transporting property, which is close to the hole transporting property of TBADN. For the aspect of electron transporting property, just as shown in **Fig. 5(b)**, 2F-DPA also exhibits the best electron transporting property among these three material, which is far better than the electron transporting property of control material of TBADN. The electron transporting property of 3F-DPA is lower than that of 2F-DPA, but higher than that of 4F-DPA significantly, which suggests that the fluorine atom on the *ortho*-position will increase the electron transporting property among these three fluorinated anthracene material. The I-V characteristic of the hole-only devices and the electron-only devices also drop a hint that the 2F-DPA may exhibit bipolar transporting ability, which was further demonstrated by the mobility test results. Just as shown in **Fig. 6**, it can be found that the hole mobility and the electron mobility of 2F-DPA are almost in the same order of 10^{-4} cm/Vs with the electric field increased from 0.2 MV/cm to 0.4 MV/cm.

In order to explore the OLED characteristics of nF-DPAs, we have fabricated non-doped blue devices, consisting of ITO/MoO_3 (3 nm)/

4,4',4"-tris-(carbazol-9-yl)-triphenylamine (TCTA) (40 nm)/Emission Layer (50 nm)/TPBi (40 nm)/LiF (1 nm)/Al (100 nm), where the nF-DPAs materials were used as emission layer respectively. The EL spectra, the current efficiency-current density characteristics, and the EQE-current density characteristics of the non-doped blue devices are shown in **Fig. 7** respectively. The device performances are summarized in **Table 2**.

As shown in **Fig. 7(a)**, compared with the control device based on TBADN with emission peak of 438 nm, devices based on nF-DPAs all exhibit deeper blue emission with the peak around 420 nm, 435 nm. The CIE of devices based on 2F-DPA, 3F-DPA, 4F-DPA, and TBADN are (0.15, 0.09), (0.15, 0.09), (0.15, 0.07), and (0.15, 0.10), respectively. As shown in **Fig.7(b)**, the peak current efficiency of devices based on the 2F-DPA, 3F-DPA, 4F-DPA, and TBADN are 1.73 cd/A, 1.61cd/A, 1.51cd/A, and 1.71 cd/A respectively. However, for the EQE performance, because of the deeper blue emission, the peak EQE of devices based on the 2F-DPA, the 3F-DPA, and the 4F-DPA, are 2.64%, 2.53%, and 2.99% ,respectively, which are higher than that of device based on TBADN (2.06%).

To study the electroluminescence performance of nF-DPAs as blue host materials, we have fabricated doped blue devices, consisting of ITO/Hexaazatriphenylenehexacabonitrile (HATCN) (5 nm)/ 4,4'-Cyclohexylidenebis[N,N-bis(4-methylphenyl)aniline] (TAPC) (40 nm)/host:dopant (7%, 20 nm)/TPBi (40 nm)/LiF (1 nm)/Al (100 nm). The nF-DPAs were used as host material respectively. Besides, device based on TBADN host material was also fabricated as control device. The doped device structure and the energy levels of the materials used in the device are shown in **Fig.8**. Here, HATCN was used as hole injection layer, and TAPC was used as hole transporting layer and exciton blocking layer, respectively.

The EL spectra, the current efficiency-current density characteristics, and the EQE-current density characteristics of all doped blue devices are shown in **Fig. 9** respectively. The device performances are summarized in **Table 3**. As shown in **Fig. 9(a)**, all doped devices based on nF-DPAs exhibit almost the same blue emission with

peaks at 473 nm and 500 nm, which is the typical EL peak of DPAVBi. The CIE coordinates of the nF-DPAs-based devices are (0.15, 0.30) at 10 V. As shown in the **Fig. 9(b)**, the peak current efficiency for device based on 2F-DPA, 3F-DPA, 4F-DPA, and TBADN are 9.6 cd/A, 8.9 cd/A, 6.7 cd/A, and 6.1 cd/A respectively. The peak EQE of doped device based on 2F-DPA, 3F-DPA, 4F-DPA, TBADN are 5.2%, 4.9%, 3.7%, and 3.4% respectively. Though the 3F-DPA material exhibits highest fluorescence quantum yield among these three nF-DPAs, OLEDs based on 2F-DPA exhibits the best efficiency performance, which may because of the balanced bipolar transporting ability of 2F-DPA.

Typically, there two opposite effect of fluoride atom on the fluorinated aromatic compounds[34]. One is the negative inductive effect. Another is the positive mesomeric effect. From the theoretical calculations results of the electronic states as well as the electrochemical properties of these three fluorinated compounds, 2F-DPA, 3F-DPA, 4F-DPA, it can be deduced that the fluoride atom at *para*-position on the phenyl ring in 4F-DPA may exhibit the strongest inductive effect, since the 4F-DPA shows the lowest HOMO and LUMO level. The fluoride atom at *ortho*-position on the phenyl ring in 2F-DPA may exhibit the most balanced state between the inductive effect and the mesomeric effect, since the 2F-DPA shows the highest HOMO and LUMO level. This balanced state will benefit the balanced bipolar charge transporting, which is also confirmed by the mobility test of 2F-DPA. Thus, it can be understand that, although the non-doped device based on 4F-DPA exhibits the best EQE performance, the doped device based on 2F-DPA shows the best efficiency performance because of the most balanced carrier property of the 2F-DPA host.

3 Conclusions

In summary, a series of efficient blue host materials of Fluorinated anthracene derivatives (nF-DPAs) have been successfully prepared by Suzuki coupling reactions in high yields. We have demonstrated that the absorption, emission, electrochemical properties, and OLED performances are significantly affected by the introduction electron-withdrawing substituent such as F. The non-doped deep blue OLED using

nF-DPAs as the emitter achieves excellent CIE coordinates of (0.15, 0.09). Moreover, the using of 2F-DPA as the host and DPAVBi as the blue-emitting dopant resulted in a high-performance OLED with a high external quantum efficiency of 5.2%, a high current efficiency of 9.6 cd A^{-1} and blue emission with a maximum luminance of over 20 000 cd m^{-2}.

4 Experimental

4.1 General information

Manipulations involving air-sensitive reagents were performed under an inert atmosphere of dry nitrogen. Commercially available reagents were used without further purification unless otherwise stated. 3-bromo-iodobenzene, anthraquinone, 2-fluorophenylboronic acid, 3-fluorophenylboronic acid, 4-fluorophenylboronic acid, n-butyllithium and tetrakis(triphenylphosphine)palladium were purchased and used as received. Absorption (UV) spectra were recorded on a Hitachi UV 3010 spectrophotometer. PL spectra were recorded on a Horiba Jobin Yvon Fluoromax-4 spectrophotometer. Glass transition temperatures (Tg) were determined with a differential scanning calorimeter (DSC, TA instruments DSC200PC) at a heating rate of 10 ^{o}C min^{-1} under a nitrogen atmosphere. Cyclic voltammetry (CV) was performed using a Princeton Applied Research model 273 A potentiostat at a scan rate of 100mV s^{-1}. All experiments were carried out in a three electrode compartment cell with a Pt-sheet counter electrode, a glassy carbon working electrode and a Pt-wire reference electrode. Reduction CV was performed in acetonitrile and oxidation CV was performed in dichloromethane with 0.1 M of tetrabutylammonium hexa-fluorophosphate as a supporting electrolyte. The potential value was recorded relative to the oxidation potential of ferrocene, which was added to the electrolyte as an internal standard. The oxidation and reduction potentials were determined by taking the average of the anodic and cathodic peak potentials.

4.2 Preparation of materials

THF (30 mL) and an aqueous solution of K_2CO_3 (2.0 M, 10 mL) were added to a flask containing 9,10-bis(3-bromophenyl)anthracene (1.74 mmol)[29], fluorinated

phenylboronic acid (10 mmol) and $Pd(PPh_3)_4$ (0.35 mmol) under nitrogen. The reaction mixture was heated to reflux and maintained at this temperature for 8 h. When the reaction was completed (judging from thin-layer chromatography), water was added to quench the reaction. Then, the products were extracted with CH_2Cl_2. The organic portion was washed with brine, dried over anhydrous $MgSO_4$, and concentrated by evaporating off the solvent. The solid was absorbed on silica gel and purified by column chromatography using light petrol ether–CH_2Cl_2 as the eluent to give the product. nF-DPAs and TBADN film samples for the film fluorescence quantum yields test ($\Phi_{f\text{-}film}$) were fabricated on the glass substrate with the thickness around 300 nm respectively. The $\Phi_{f\text{-}film}$ was measured by PTi-Q40 fluorescence spectrophotometer with a calibrated integrating sphere.

4.2.1 9,10-Bis-(2'-fluoro-biphenyl-3-yl)-anthracene (2F-DPA). 0.71 g, white solid, yield: 83%. ^{1}H-NMR (DMSO, 400 MHz) δ: 7.819-7.803 (d, 2H), 7.652-7.717 (m, 8H), 7.528-7.559(t, 4H), 7.471-7.496 (m, 6H), 7.314-7.374(t, 4H). Anal calcd for $C_{38}H_{24}F_2$: C, 88.04; H, 4.63. Found: C, 88.01; H, 4.62%.

4.2.2 9,10-Bis-(3'-fluoro-biphenyl-3-yl)-anthracene (3F-DPA). 0.73 g, white solid, yield: 85%. ^{1}H-NMR (DMSO, 400 MHz) δ: 7.985-8.003 (d, 2H), 7.779-7.863 (m, 4H), 7.648-7.697 (m, 8H), 7.459-7.548 (m, 6H), 7.209-7.248 (t, 4H). Anal calcd for $C_{38}H_{24}F_2$: C, 88.04; H, 4.63. Found: C, 88.02; H, 4.60%.

4.2.3 9,10-Bis-(4'-fluoro-biphenyl-3-yl)-anthracene (4F-DPA). 0.67 g, white solid, yield: 79%. ^{1}H-NMR (DMSO, 400 MHz) δ: 7.926-7.939 (d, 2H), 7.826-7.861 (m, 4H), 7.761-7.799 (m, 4H), 7.675-7.700 (m, 4H), 7.455-7.480 (m, 6H), 7.283-7.332 (t, 4H). Anal calcd for $C_{38}H_{24}F_2$: C, 88.04; H, 4.63. Found: C, 87.98; H, 4.59%.

4.3 Device fabrication and testing

All of the organic materials were purified by temperature gradient sublimation in a vacuum. The devices were fabricated by conventional vacuum deposition of the organic layers, LiF and an Al cathode onto an ITO-coated glass substrate under a base pressure lower than 10^{-3} Pa. The thickness of each layer was determined by a quartz thickness monitor. The voltage–current density (*V*–*J*) and voltage–brightness (*V*–*L*) as

well as the current density–current efficiency (J–η_c) and current density–power efficiency (J–η_p) curve characteristics of the devices were measured with a Keithley 2602 and Source Meter. All measurements were carried out at room temperature under ambient conditions.

Acknowledgements

We thank the Pro. Duan Lian and Dr. Bin Zhengyang (Key Lab of Organic Optoelectronics and Molecular Engineering of Ministry of Education, Department of Chemistry, Tsinghua University) for the the measurement of holes and electrons mobility of our materials. We also thank the Dr. Ye Honggang (School of Science, Xi'an Jiaotong University) for the measurement of the fluorescence quantum yields of nF-DPA films. This work was financially supported by Basic Research Program of China (2013CB328705), National Natural Science Foundation of China (Grant Nos. 61275034, 61106123), Ph.D. Programs Foundation of Ministry of Education of China (Grant No. 20130201110065).

Reference

1 C. W. Tang and S. A. VanSlyke, Appl. Phys. Lett., 1987, 51, 913.

2 L. S. Hung and C. H. Chen, Mater. Sci. Eng., R, 2002, 39, 143.

3 S. R. Forrest, Nature, 2004, 428, 911.

4 L. M. Leung, W. Y. Lo, S. K. So, K. M. Lee and W. K. Choi, J. Am. Chem. Soc., 2000, 122, 5640.

5 S. Tang, M. Liu, P. Lu, H. Xia, M. Li, Z. Xie, F. Shen, C. Gu, H. Wang, B. Yang and Y. Ma, Adv. Funct. Mater., 2007, 17, 2869.

6 C. H. Wu, C. H. Chien, F. M. Hsu, P. I. Shih and C. F. Shu, J. Mater. Chem., 2009, 19, 1464.

7 C. W. Tang, S. A. VanSlyke and C. H. Chen, J. Appl. Phys., 1989, 65, 3610.

8 Y. H. Kim, D. C. Shin, S. H. Kim, C. H. Ko, H. S. Yu, Y. S. Chae and S. K. Kwon, Adv. Mater., 2001, 13, 1690.

9 J. Shi and C. W. Tang, Appl. Phys. Lett., 2002, 80, 3201.

10 Y. Kan, L. Wang, L. Duan, Y. Hu, G. Wu and Y. Qiu, Appl. Phys. Lett., 2004, 84, 1513.

11 C. Hosokawa, H. Higashi, H. Nakamura and T. Kusumoto, Appl. Phys. Lett., 1995, 67, 3853.

12 K. C. Wu, P. J. Ku, C. S. Lin, H. T. Shih, F. I. Wu, M. J. Huang, J. J. Lin, I. C. Chen and C. H. Cheng, Adv. Funct. Mater., 2008, 18, 67.

13 C. C. Wu, Y. T. Lin, K. T. Wong, R. T. Chen and Y. Y. Chien, Adv. Mater., 2004, 16, 61.

14 T. C. Chao, Y. T. Lin, C. Y. Yang, T. S. Hung, H. C. Chou, C. C. Wu and K. T. Wong, Adv. Mater., 2005, 17, 992.

15 L. H. Chan, H. C. Yeh and C. T. Chen, Adv. Mater., 2001, 13, 1637.

16 S. J. Lee, J. S. Park, K. J. Yoon, Y. I. Kim, S. H. Jin, S. K. Kang, Y. S. Gal, S. Kang, J. Y. Lee and J. W. Kang, Adv. Funct. Mater., 2008, 18, 3922.

17 C. J. Tonzola, A. P. Kulkarni, A. P. Gifford, W. Kaminsky and S. A. Jenekhe, Adv. Funct. Mater., 2007, 17, 863.

18 A. P. Kulkarni, A. P. Gifford, C. J. Tonzola and S. A. Jenekhe, Appl. Phys. Lett., 2005, 86, 061106.

19 K. Danel, T. H. Huang, J. T. Lin, Y. T. Tao and C. H. Chuen, Chem. Mater., 2002, 14, 3860.

20 W. J. Shen, R. Dodda, C. C. Wu, F. I. Wu, T. H. Liu, H. H. Chen, C. H. Chen and C. F. Shu, Chem. Mater., 2004, 16, 930.

21 S. Tao, Z. Hong, Z. Peng, W. Ju, X. Zhang, P. Wang, S. Wu and S. Lee, Chem. Phys. Lett., 2004, 397, 1.

22 S. K. Kim, B. Yang, Y. Ma, J. H. Lee and J. W. Park, J. Mater. Chem., 2008, 18, 3376.

23 P. I. Shih, C. Y. Chuang, C. H. Chien, E. W. G. Diau and C. F. Shu, Adv. Funct. Mater., 2007, 17, 3141.

24 Y. H. Kim, D. C. Shin, S. H. Kim, C. H. Ko, H. S. Yu, Y. S. Chae and S. K. Kwon, Adv. Mater., 2001, 13, 1690.

25 Y. H. Kim, H. C. Jeong, S. H. Kim, K. Yang and S. K. Kwon, Adv. Funct. Mater., 2005, 15, 1799.

26 S. Tao, Y. Zhou, C. S. Lee, S. T. Lee, D. Huang and X. Zhang, J. Phys. Chem. C, 2008, 112, 14603.

27 J. J. Oh, Y. J. Pu and Junji Kido, Chem. Lett., 2011, 40, 1092.

28 M. Zhu, Q. Wang, Y. Gu, X. S. Cao, C. Zhong, D. G. Ma, J. G. Qin and C. L. Yang, J. Mater. Chem., 2011, 21, 6409.

29 Y. D. Sun, L. Duan, D. Q. Zhang, J. Qiao, G. F. Dong, L. D. Wang and Y. Qiu, Adv. Funct. Mater., 2011, 21, 1881.

30 J. Cornil, N. E. Gruhn, D. A. Dos Santos, M. Malagoli, P. A. Lee, S. Barlow, S. Thayumanavan, S. R. Marder, N. R. Armstrong and J. L. Br´edas, J. Phys. Chem. A, 2001, 105, 5206.

31 Z. Li, Z. Wu, B. Jiao, P. Liu, D. Wang and X. Hou, Chem. Phys. Lett., 2012, 527, 36.

32 J. S. Reddy, T. Kale, G. Balaji, A. Chandrasekaran and S. Thayumanavan, J. Phys. Chem. Lett., 2011, 2, 648.

33 M. L. Tang and Z. Bao, Chem. Mater., 2011, 23, 446.

34 F. Babudri, G. M. Farinola, F. Naso and R. Ragni, Chem. Commun., 2007, 1003.

35 Z. Li, Z. Wu, W. Fu, P. Liu, B. Jiao, D. Wang, G. Zhou and X. Hou, J. Phys. Chem. C, 2012, 116, 20504.

36 K. Reichenb¨acher, H. I. S¨uss and J. Hulliger, Chem. Soc. Rev., 2005, 34, 22.

37 R. Berger, G. Resnati, P. Metrangolo, E. Weber and J. Hulliger, Chem. Soc. Rev., 2011, 40, 3496.

38 Y. Tao, Q. Wang, Y. Shang, C. Yang, L. Ao, J. Qin, D. Ma and Z. Shuai, Chem. Commun., 2009, 77.

39 C.H. Wu, C.H. Chien, F.M. Hsu, P.I. Shih and C.F. Shu, J. Mater. Chem., 2009, 19, 1464.

40 J. Salbeck, N. Yu, J. Bauer, F. Weissortel and H. Bestgen, Synth. Met., 1997, 91, 209.

41 A. Thangthong, D. Meunmart, N. Prachumrak, S. Jungsuttiwong, T. Keawin, T. Sudyoadsuk and V. Promarak, Chem. Commun., 2011, 47, 7122.

42 Z. F. Li, Z. X. Wu, W. Fu, P. Liu, B. Jiao, D. D. Wang, G. J. Zhou and X. Hou, J. Phys. Chem. C., 2012, 116, 20504.

43 T. Zhou, F. Li, Y. Fan, W. Song, X. Mu. H. Zhang, and Y. Wang, Chem. Commun., 2009,3199.

Tables

Table 1. Optical, thermal, and electrochemical properties of the compounds.

Compound	$\lambda_{max}^{Abs\ a/b}$ (nm)	$\lambda_{max}^{PL\ a/b}$ (nm)	T_g/T_d [c] (°C)	$\Phi_{f\text{-}sol}$ [d]/$\Phi_{f\text{-}film}$	E_{ox} [e] (V)	HOMO/LUMO^{exp} (E_g^{opt}) [f] (eV)	HOMO/LUMO^{cal} ($\Delta E_{HOMO\text{-}LUMO}$)[g] (eV)
2F-DPA	280,340,355,375,395 /290,345,360,380,400	433,461/ 421,440	117/385	0.49/0.36	0.92	–5.72/–2.72 (3.0)	–5.04/–1.57(3.47)
3F-DPA	280,340,355,375,395 /290,345,360,380,400	433,461/ 421,440	112/385	0.52/0.41	0.99	–5.79/–2.79 (3.0)	–5.19/–1.70 (3.49)
4F-DPA	280,340,355,375,395 /290,345,360,380,400	433,461 /421,440	119/385	0.51/0.38	1.02	–5.82/–2.82(3.0)	–5.20/–1.71(3.49)

[a] Measured in CH_2Cl_2. [b] Measured in solid thin film on quartz plates. [c] T_g: glass-transition temperature; T_d: thermal-decomposition temperatures ; NA: not available. [d] Determined in CH_2Cl_2 using quinine sulfate (Φ_{PL} = 0.56 in 1.0 M H_2SO_4 solution) as standard. [e] Determined from the onset of oxidation potentials; measured in CH_2Cl_2; [f] The HOMO and LUMO energies were determined from cyclic voltammetry and the absorption onset. $E_{HOMO} = -(qE_{ox} + 4.8)$ eV; $E_{LUMO} = E_{HOMO} + E_g^{opt}$. [g] Values from DFT calculation.

Table 2. The performance of non-doped devices.

EML	$\lambda_{max}^{EL\ a}$ (nm)	V_{on} [b] (V)	L_{max} [c] (cd m^{-2})	η_c [d] (cd A^{-1})	η_p [d] (lm W^{-1})	EQE[d] (%)	CIE (x, y) [a]
2F-DPA	420,435	3.77	3557	1.73	1.26	2.64	(0.15, 0.09)
3F-DPA	420,435	4.28	2518	1.61	1.08	2.53	(0.15, 0.09)
4F-DPA	420,435	5.66	1503	1.51	0.71	2.99	(0.15, 0.07)
TBADN	438	3.26	4428	1.71	1.58	2.06	(0.15, 0.10)

[a] Values collected at 10 V. [b] Turn-on voltage at 1 cd m^{-2}. [c] Maximum luminance. [d] Values collected at a peak efficiency.

Table 3. EL performance of nF-DPAs-doped devices

EML	$\lambda_{max}^{EL\ a}$ (nm)	V_{on} [b] (V)	L_{max} [c] (cd m^{-2})	η_c [d] (cd A^{-1})	η_p [d] (lm W^{-1})	*EQE* (%)	CIE (x, y) [a]
2F-DPA: DPAVBi(7%)	473,500	2.8	27638	9.6	7.7	5.2	(0.15, 0.30)
3F-DPA: DPAVBi(7%)	473,500	3.2	14639	8.9	5.3	4.9	(0.15, 0.30)
4F-DPA: DPAVBi(7%)	473,500	3.4	11277	6.7	3.9	3.7	(0.15, 0.30)
TBADN: DPAVBi(7%)	473,500	3.0	17121	6.1	5.1	3.4	(0.15, 0.30)

[a] Values collected at 10 V. [b] Turn-on voltage at 1 cd m^{-2}. [c] Maximum luminance. [d] Values collected at a peak efficiency.

FIGURE LEGENDS

Scheme 1 Synthetic scheme of nF-DPAs.

Fig 1. The molecular orbital surfaces of the HOMOs and LUMOs for the nF-DPAs obtained at the B3LYP/6-31G level**.**

Fig 2. DSC **(a)** and TGA **(b)** of nF-DPAs.

Fig 3. Absorption of nF-DPAs in CH_2Cl_2 **(a) and** in films **(b)**, PL spectra of nF-DPAs in CH_2Cl_2 **(c)** and in films **(d)**. Absorption and PL spectra of DPAVBi in films **(d)**.

Fig 4. Cyclic voltammograms of nF-DPAs in CH_2Cl_2.

Fig 5. The hole-only **(a)** and electron-only **(b)** device.

Fig 6. Electron and hole mobilities versus $E^{1/2}$ for 2F-DPA.

Fig 7. EL spectra measured at 10 V (a), current efficiency-current density characteristics (b), and external quantum efficiency-current density characteristics (c) for the non-doped devices with the structure of ITO/MoO_3/TCTA/EML/TPBi/LiF/Al, where the EML is 2F-DPA, 3F-DPA, 4F-DPA, and TBADN respectively.

Fig 8. Energy-level diagram of the doped devices.

Fig 9. The EL spectra at 10 V **(a)**, Current Efficiency-current density curves **(b)** and EQE-current density curves **(c),** for the doped devices with the structure of ITO/HATCN/TAPC/Host:Dpavbi/TPBi/LiF/Al, where the host is 2F-DPA, 3F-DPA, 4F-DPA, and TBADN respectively.

Scheme 1

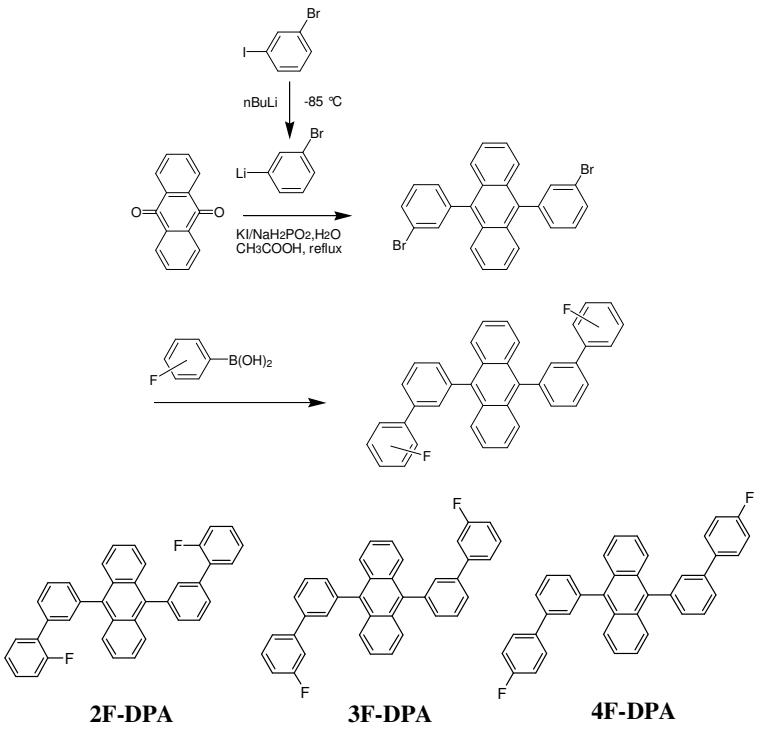

Fig 1.

Compound	HOMO	LUMO
2F-DPA	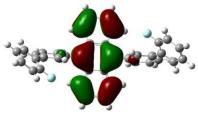	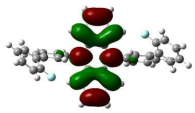
3F-DPA	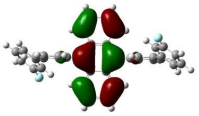	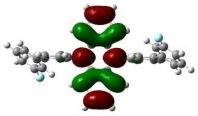
4F-DPA	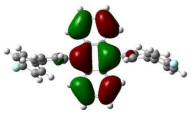	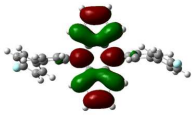

Fig 2.

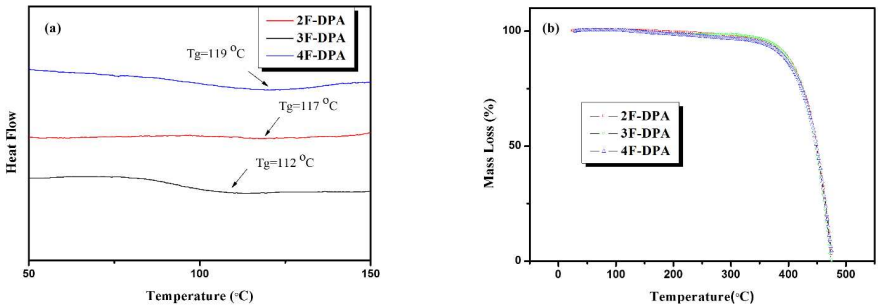

Fig 3.

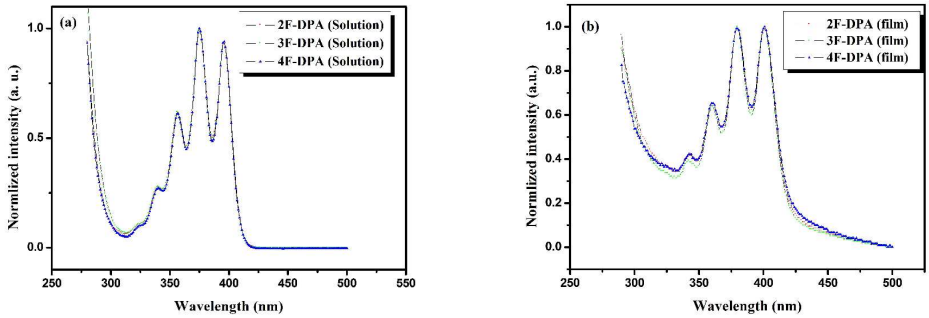

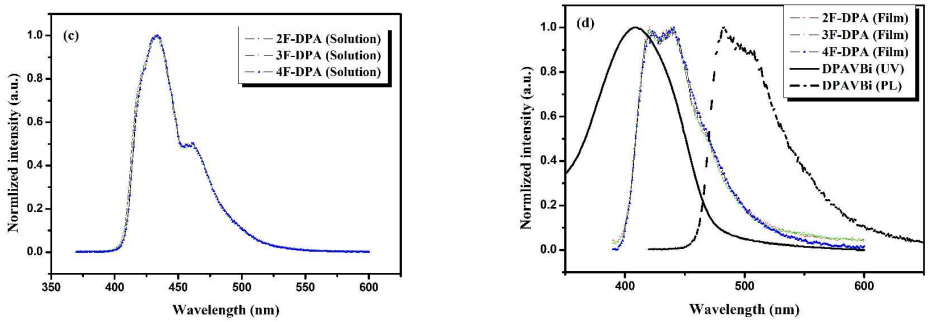

Fig 4

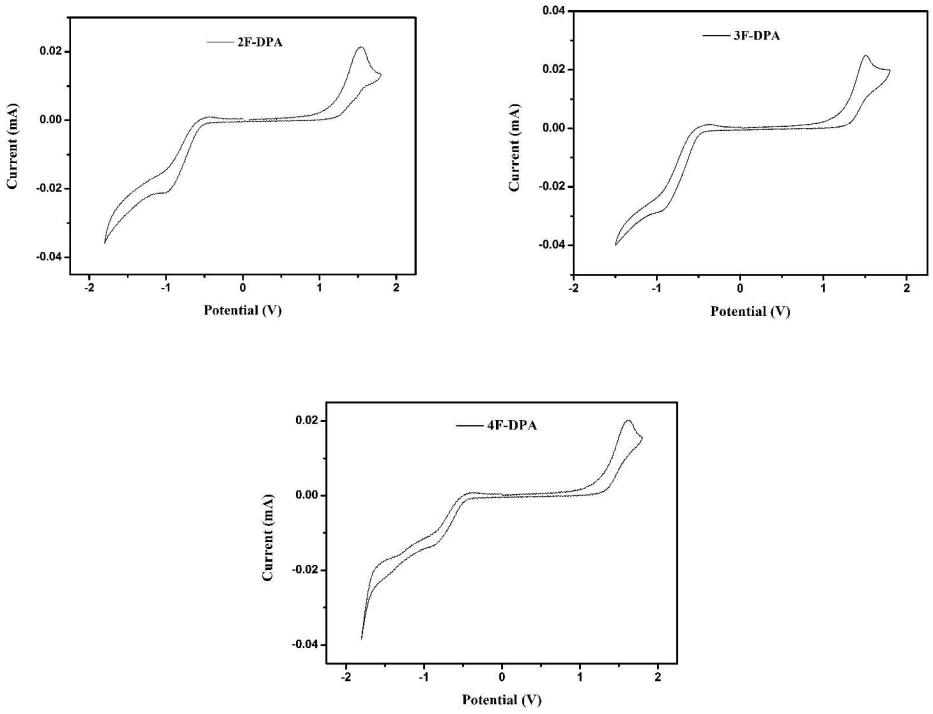

Fig 5

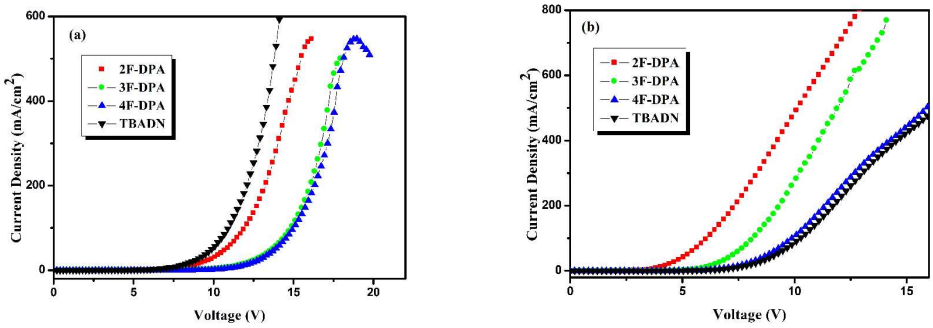

Fig 6

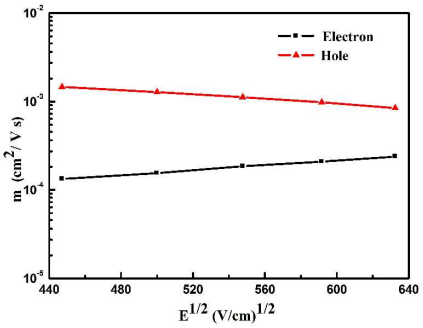

Fig 7.

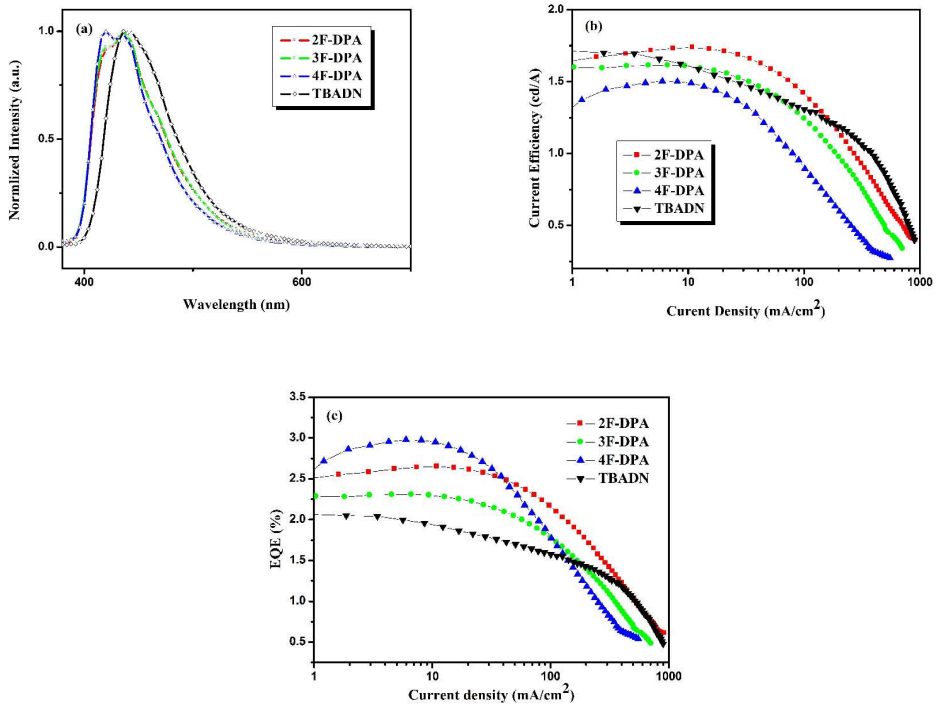

Fig 8.

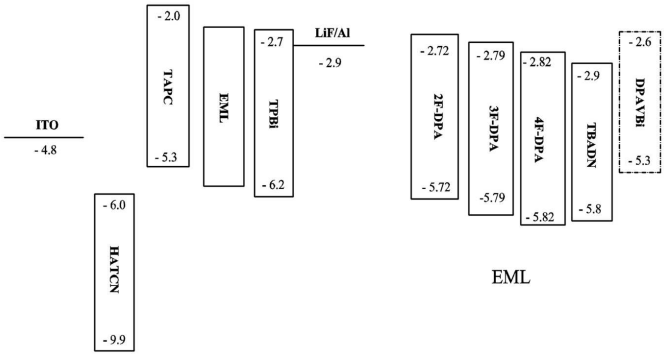

Fig 9.